Experimental evaluation of the operating temperature impact on solid oxide anode-supported cells

Pierluigi Leone

Politecnico di Torino, Dipartimento di Energetica

C.so Duca Degli Abruzzi 24, 10100
Torino, Italy

Pietro Asinari

Politecnico di Torino, Dipartimento di Energetica

C.so Duca Degli Abruzzi 24, 10100
Torino, Italy

Massimo Santarelli

Politecnico di Torino, Dipartimento di Energetica

C.so Duca Degli Abruzzi 24, 10100
Torino, Italy

Michele Calì

Politecnico di Torino, Dipartimento di Energetica

C.so Duca Degli Abruzzi 24, 10100
Torino, Italy

ABSTRACT

In this paper an experimental investigation on single planar solid oxide cells is presented. Tests were performed on SOFCs of anode-supported design at L.A.Q. IN.T.E.SE laboratory of Politecnico di Torino where a test facility was installed. In the paper results are presented concerning the characterization of planar circular-shaped cells from InDEC® with LSM and LSCF cathodes. The characterization was performed by taking V-I measurements over a range of temperatures between 650°C and 840°C with hydrogen as fuel, and air as oxidant. The dependence of the cell performance on the various polarization contributions was rationalized on the basis of a simple analytical model, through a parameter estimation on the experimental data.
The apparent thermal activation energy E_a has been evaluated from the temperature dependence of ASRs. The cell with LSCF cathode has a lower activation energy and thus it is suitable for operating temperature lower than ASC1 cell one. The fuel cell performance dependence on the temperature is due to the temperature dependence of ohmic and activation polarization. In particular, the performance limitation at low temperature is due to activation polarization for ASC1 and ohmic polarization for ASC2.

Key words*:* SOFC single cells, experimental, performance limitation, temperature impact

1. INTRODUCTION

In this paper an experimental analysis on single planar SOFC units is presented. Tests were performed on solid oxide fuel cells of anode-supported design at L.A.Q. IN.T.E.SE laboratory of Politecnico di Torino. In the paper results are presented concerning the characterization of anode-supported cells with LSM and LSCF cathodes. Experimental data analysis consisted in the definition and evaluation of performance indexes of cells such as maximum power density, current

density at 0.7 volts, area specific resistance analysis and polarization analysis coupled with parameter estimation methods[1-10].

Lanthanum–strontium manganite (LSM) is known to be the most promising candidate for practical SOFC cathode, due to mechanical and chemical compatibility with zirconia electrolyte and good electrochemical performances at 1000 °C. However, its polarization property at lower temperatures (≤800 ◦C) is not satisfactory.

The medium-temperature performance can be enhanced when a second ionically conducting phase is added to LSM to extend the surface area over which the oxygen reduction reaction can occur. Very good results were obtained using a LSM–YSZ cathode

Iron and cobalt-containing perovskites (LSCF) are other candidates for SOFC cathode materials, because of their high electronic and ionic conductivity as well as high oxygen permeability and high electrocatalytic activity.

It is important to note that in the case of pure electronic conducting cathode materials (like lanthanum–strontium manganite is at medium-temperatures) the electrochemical reactions are almost restricted to the triple phase boundary between the cathode, electrolyte and gaseous oxygen or air. On the other side, LSCF cathodes, referred as Mixed Electronic and Ionic Conductors (MEIC), have appreciable ionic conductivity, and exchange of oxygen occurs at the electrode surface with diffusion of oxygen ions through the mixed conductor [6, 7].

Several research group investigated the different behaviour of single cell operation with YSZ/LSM and LSCF cathodes. In [8] authors investigate properties and the applicability of iron and cobalt-containing perovskites as cathodes for solid oxide fuel cells (SOFCs) in comparison to state-of-the-art manganite-based perovskites. In comparison with the performance of a state-of-the-art LSM/YSZ composite cathode, the current densities of the better performing LSCFs (L55SCF, L58SCF, L78SCF) are up to two times higher than for the LSM cathode, Further, LSCF cathodes gave a power output of 1.0–1.2 Wcm^{-2} at 800 °C and 0.7 Volts with hydrogen as fuel gas, compared with conventional cathodes based on $(La,Sr)MnO_3$ (LSM), the high power densities allow a reduction in operating temperature of about 100 °C by maintaining the performance at the former level with LSM cathodes. In [9] the electrochemical performance of different LSCF-based cathodes in comparison to the state-of-the-art LSM cathodes was also considered. Focusing on the temperature dependence, it was found that the higher electro-catalytic activity of the LSCF compositions becomes evident in comparison to LSM. The difference in performance between the various LSCF compositions is nearly the same for 800 and 700 °C, while the performance of the LSM/YSZ cells has a stronger temperature dependence, resulting in a stronger increase of overpotential with decreasing temperature. In [10] it is presented a screening of different cathode properties for application in low-temperature SOFC technology. Basing on impedance spectroscopy analysis on symmetrical cells it was found a polarization resistance of 0.5 Ω cm^2 for LSM cathode at around 760 °C, at 650 °C for LaSrFeCo.

2. EXPERIMENTAL

The tests were performed with circular shaped anode supported SOFC membranes from InDEC®, with a diameter of 80 mm and an active area of 47 cm^2.

Cells were of anode-supported design, two kinds of cells were tested differing for the materials used in the cathode layer. First cell is referred as ASC1 cell. The electrolyte of these membranes was 4-6 µm thick 8YSZ. The cathode was 30-40 µm thick and consisted of two layers. The cathode functional layer consisted of porous 8YSZ and $La_{0.75}Sr_{0.2}MnO_3$ (LSM). The cathode current collecting layer consisted of LSM alone. The anode consisted of two layers. Both functional layers and support consisted

of nickel and 8YSZ. The anode support was 520-600 µm and the functional layer 5-10 µm. The second design of cell is referred as ASC2 cell. The electrolyte of these membranes was 4-6 µm thick 8YSZ. The cathode consisted of a 2-4 µm thick of blocking layer made of yttria doped ceria (YDC) and 20-30 µm thick of functional layer consisted of porous lanthanum strontium cobalt ferrite oxide (LSCF). The anode was the same of the ASC1 design.

The membranes were tested in a ceramic cell housing, with alumina flanges for gas distribution, platinum gauze for cathode current collection, and nickel gauze for anode current collection. The anode and cathode chambers were not sealed, allowing the fuel to react with oxygen directly outside the fuel cell. Platinum wires were used as current leads and for cell voltage measurement. As fuel flow, hydrogen was used. The fuel was humidified by a bubbler operating at 30°C. The flows were controlled by mass flow controllers (Bronkhorst). The V-j characteristics were taken changing current in steps of 1 A, and stabilisation time at each step of 60 seconds, by using a Kikusui electronic load (Kikusui Electronics Corp, Japan) in conjunction with an additional power supply in current-following mode (Delta Elektronica, Zierikzee, Netherlands).

The experimental session mainly consisted of comparison of different polarization behavior changing the anodic feeding in terms of hydrogen mass flow. Also the effect of the cell temperature was evaluated with SOFC membranes at 650 °C , 740°C ,800°C and 840°C.

3. SINGLE CELL UNIT TEST RESULTS: PERFORMANCE INDEXES ANALYSIS

An analysis of cell operation was accomplished by defining suitable performance indexes of operation.

Essentially these indexes refer to power-generating characteristics of unit-cells, area specific resistance analysis and polarization analysis.

3.1. Polarization analysis: power-generating characteristics of unit-cells

3.1.1. Anode Supported cell with YSZ/LSM cathode (ASC1)

In Figure 1 the measured *V-i* curves are drawn for the temperature of 800 °C with the power density curves of the cell. The cell resistances R_{cell}, evaluated from the linear region of V(*i*) versus j curves are 8.08mΩ, 8.58mΩ and 9.67mΩ for 500 mln/min H_2, 400 mln/min H_2 and 300 mln/min H_2. The cell electrical powers achieved at 0.7 volts were 25 W at 50.2% fuel utilization (500 mln/min H2), 22.5 W at 56.3% fuel utilization (400 mln/min H2) and 19.63 W at 65.7% fuel utilization (300 mln/min H2). The maximum power densities (MPD) have been ~577 mW/cm^2 507 mW/cm^2 and 429 mW/cm^2.

3.1.2. Anode Supported cell with YDC/LSCF cathode (ASC2)

In Figure 2 the measured *V-i* curves are drawn for the temperature of 800 °C with the power density curves of the cell. The cell resistances R_{cell}, evaluated from the linear region of V(*i*) versus *i* curves are 5.06mΩ, 5.63mΩ and 6.83mΩ for 500 mln/min H_2, 400 mln/min H_2 and 300 mln/min H_2. The cell electrical powers achieved at 0.7 volts were 32 W at 64% fuel utilization (500 mln/min H_2), 29.1

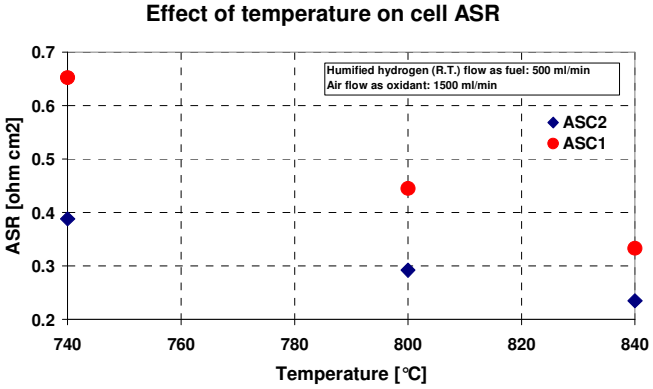

Figure 5. Effect of operating temperature on the Area Specific Resistance (ASR)

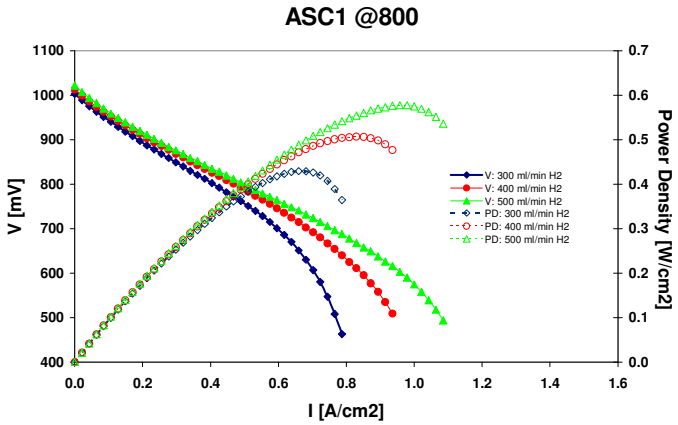

Figure 1. Power-generating characteristics of unit-cells, Anode Supported cell with YSZ/LSM cathode (ASC1) at 800°C.

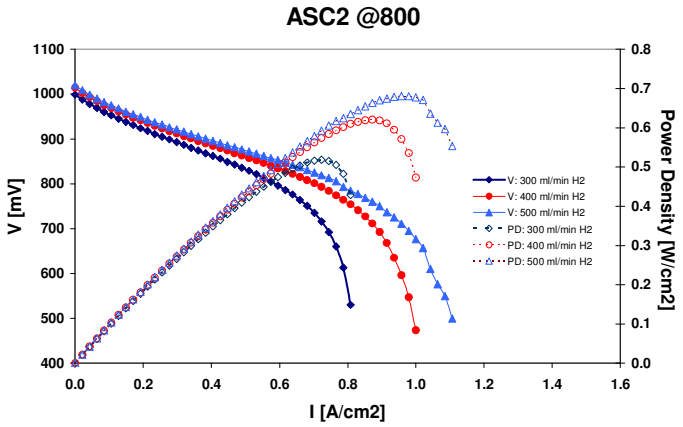

Figure 2. Power-generating characteristics of unit-cells, Anode Supported cell with YDC/LSCF cathode (ASC2) at 800 °C.

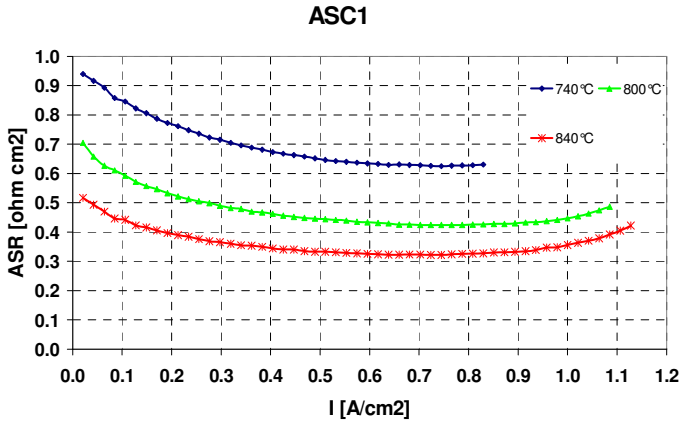

Figure 3. Area Specific Resistance of ASC1 cell.

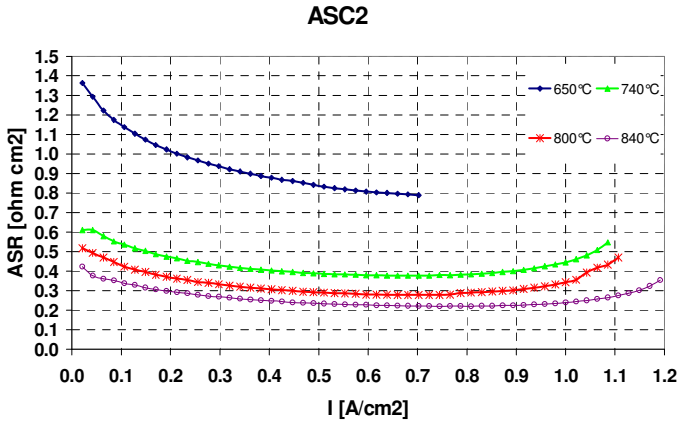

Figure 4. Area Specific Resistance of ASC2 cell.

W at 73% fuel utilization (400 mln/min H_2), 24.2 W at 82% fuel utilization (300 mln/min H2). The maximum power densities (MPD) have been ~681 mW/cm^2, 620 mW/cm^2 and 518 mW/cm^2.

For all the investigated temperatures the cell resistances decrease as the anode feed rate is increased because of the reduction of gas c onversion resistance. Also, the increase of temperature leads to the reduction of cell resistance due increase of rate of electrochemical reaction and decrease of ohmic overpotentials.

3.2. Polarization analysis: Area Specific Resistance (ASR) Analysis

The overall cell performance obtained from the V-I characteristics for both types of unit-cell at various operation conditions is presented in Figures 3, Figures 4, Figures 5.
The cell performance is estimated in terms of the area specific resistance of the cell (ASR) rather then power density, which is more often employed as suitable index to represent overall cell performance. In fact, this description of cell performance is known to be much less dependent on the individual test conditions compared with power density [1, 2, 11]. This parameter is representative of total cell polarization.

In this work the area specific resistance was evaluated as [1]:

$$ASR = \frac{OCV - V_{cell}}{j} \quad (1)$$

Where OCV is the experimental open circuit voltage, V_{cell} is the measured cell voltage and j the corresponding current. In Figures 5 it is possible to evaluate the effect of temperature and fuel utilization on the area specific resistance. Total cell resistance is less dependent of temperature in case of ASC2 than in case of ASC1.

3.3. Electrochemical Investigation of cell performance

In this paragraph the polarization analysis is refined by describing a cell polarization model and fitting the experimental data through parameter estimation methods. The polarization analysis was performed for the two cells, at different operating temperatures and at fixed fuel mass flow of 500 ml/min (nominal condition). The considered polarization model is defined and discussed in the following. The model equation used in the paper is described in following equations. The terminal cell voltage is expressed by the following equation:

$$V_c = V_{Nernst} - \frac{R\cdot T}{\alpha\cdot F} a\sinh\left(\frac{i_c}{2\cdot I_{0,c}}\right) - R_\Omega \cdot i_c + \frac{R\cdot T}{2\cdot F}\log\left(1-\frac{i}{i_{as}}\right) + \frac{R\cdot T}{4\cdot F}\log\left(1-\frac{i}{i_{cs}}\right) \quad (2)$$

The Nernst potential, V_{Nernst} has been assumed equal to the measured open circuit voltage. The activation overvoltage has been modelled using a single-term equation of the hyperbolic sine approximation of Butler-Volmer equation. This is equal to assume one of the equilibrium exchange current densities sufficiently larger than the other, thus allowing the corresponding activation loss to be neglected [11]. The ohmic resistance is modelled considering a global resistance of electrolyte, electrodes and any contact resistance between interfaces and between current collectors. The resistance of 8YSZ electrolyte has been modeled using the equation:

$$\rho_{el} = 0.00294\cdot e^{\left(\frac{10350}{T}\right)} \quad (3)$$

In terms of physical measurable parameters, an analytical expression for the anode diffusion overpotential is proposed [3]. The expression of the limiting current density at the anode side is:

$$i_{as} = \frac{2\cdot F\cdot p^b_{H_2}\cdot D_{a(eff)}}{R\cdot T\cdot t_a} \quad (4)$$

The effective diffusion coefficients have been evaluated according to the equation:

$$D_{a/c(eff)} = \frac{\varepsilon_{a/c}}{\tau_{a/c}}\cdot D^{293K}_{i-j}\cdot\left(\frac{T}{293}\right)^{1.5} \quad (5)$$

The diffusion overpotential due to the anode diffusion is then given by:

$$V^a_{diff} = \frac{R\cdot T}{2\cdot F}\log\left(1-\frac{i}{i_{as}}\right) \quad (6)$$

In terms of physical measurable parameters, the cathode limiting current density was evaluated with equation [3]:

$$i_{cs} = \frac{4\cdot F\cdot p^b_{O_2}\cdot D_{c(eff)}}{\left(\frac{p-p^b_{O_2}}{p}\right)\cdot R\cdot T\cdot t_c} \quad (7)$$

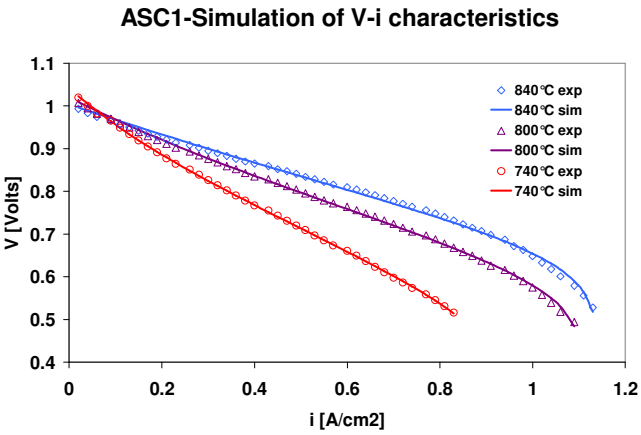

Figure 6. Experimental versus polarization behavior of anode-supported cell with SLM cathode

(This equation is an approximation for anode supported cells with very small cathode thickness). The diffusion overvoltage due to the cathode diffusion is then given by:

$$V_{diff}^{c} = \frac{R \cdot T}{4 \cdot F} \log\left(1 - \frac{i}{i_{cs}}\right) \quad (8)$$

The effective diffusion coefficients have been evaluated according to the equation (5),where the fundamental binary diffusivity of reactants mixtures are evaluated according to the Chapman-Enskog model [3, 4, 12, 13]. Three parameters were estimated in the analysis, 1) the effective exchange current density $I_{0,c}$, 2) the global ohmic resistance R_{Ω} and 3) the anode limiting current density i_{as}. Parameter estimation was performed using Levenberg-Marquardt algorithm, results are shown in Table 1. In Figure 6 an example of parameter estimation procedure is drawn with experimental and fitting *V-j* curves.

The ohmic polarization is temperature dependent mainly because the thermally activated dependence of the YSZ ionic resistivity. The activation polarization is also thermally activated, which is reflected in the thermally activated dependence of the exchange current density $I_{o,c}$, in fact the cathode exchange current densities increase at the increase of temperature with meaning of reduction of electrode polarization at high temperature. Also ohmic resistance decrease at the increase of temperature with exponential behavior. Anode limiting current densities slightly varies with temperature as expected. Further, as temperature was decreased worst estimations of anode limiting current densities were obtained suggesting that at low temperature other sources of polarization, rather than concentration, limit the cell performance. Thus, the principal temperature dependence of cell performance is due to the temperature dependence of ohmic and activation polarization.

At 800 °C values of cathode exchange current densities of around 110 mA/cm^2 and 170 mA/cm^2 were found for ASC1 cell and for the ASC2 cell, respectively. In general the estimated values of global ohmic resistances are higher than the model value of ionic resistance of electrolyte, this means that there is an important contribution of ohmic resistance which arises from other sources such as electrode resistance, resistance of interfaces, contact resistance.

Anode limiting current densities slightly varies for the two investigated cells because the anode was of same material and design. Concentration overvoltages evaluated in this analysis are strongly dependent with operating conditions and include contribution of conversion resistance (fuel utilization effect).

4. COMPARISON OF LIMITING PERFORMANCE FACTORS OF CELLS

4.1. Performance Index Analysis

In Figure 7 V-I characteristics of ASC1 and ASC2 cells are drawn for 500 ml/min of hydrogen and for different operating temperatures. The current-voltage behavior of ASC2 at 740°C is comparable with performance of ASC2 at 840 °C. In particular from the Figure 8 it is possible to understand the behavior of cells at different temperatures and thus roughly characterize the behavior of the improved cathode for different operating temperatures. At 740 °C and 500 ml/min of

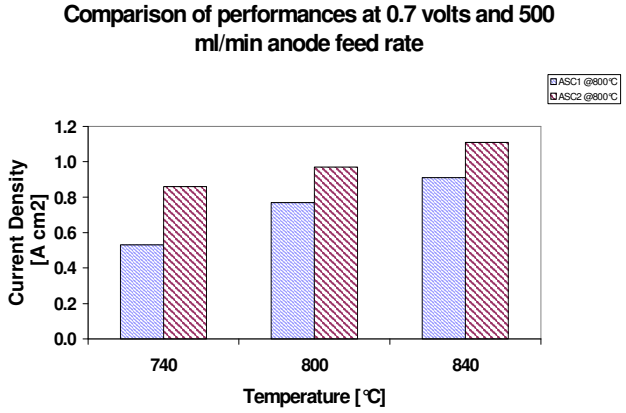

Figure 8. Comparison of cell performances in terms of temperature effect

	ASC1	840	ASC2	840
	Estimation	Δ,condifence interval	Estimation	Δ,condifence interval
$I_{o,c}$ [A/cm^2]	0.197	±0.031	0.236	±0.045
R_Ω [ohm cm^2]	0.135	±0.013	0.048	±0.014
I_{as} [A/cm^2]	1.144	±0.005	1.196	±0.002
	ASC1	800	ASC2	800
	Estimation	Δ,condifence interval	Estimation	Δ,condifence interval
$I_{o,c}$ [A/cm^2]	0.112	±0.009	0.168	±0.032
R_Ω [ohm cm^2]	0.189	±0.008	0.081	±0.017
I_{as} [A/cm^2]	1.113	±0.006	1.066	±0.002
	ASC1	740	ASC2	740
	Estimation	Δ,condifence interval	Estimation	Δ,condifence interval
$I_{o,c}$ [A/cm^2]	0.060	±0.003	0.147	±0.024
R_Ω [ohm cm^2]	0.322	±0.009	0.174	±0.014
I_{as} [A/cm^2]	0.938	±0.020	1.050	±0.004
	ASC1	650	ASC2	650
	Estimation	Δ,condifence interval	Estimation	Δ,condifence interval
$I_{o,c}$ [A/cm^2]	NP	NP	0.041	±0.003
R_Ω [ohm cm^2]	NP	NP	0.508	±0.030
I_{as} [A/cm^2]	NP	NP	1.275	±0.510

Table 1. Estimated parameters of polarization model for ASC1 and ASC2 cells

fuel the voltage of 0.7 volts is reached at a double value of current density in the case of ASC2. Increasing the temperature the positive effect of the improved cathode decreases.

4.2. Thermal Activated Process Analysis

A comparison of cell behavior in terms of polarization and effect of temperature has been done. In fact, the apparent thermal activation energy Ea has been evaluated from the temperature dependence of ASRs. In particular for the ASC1 cell an apparent thermal activation energy of around 0.65 eV has been estimated. Contrary we evaluated for the ASC2 cell a value of Ea of around 0.48 eV. Further, the Ea, referred to the ohmic resistances, of ASC1 is lower than the one of ASC2 (0.94 and 1.34 eV respectively), whereas the activation energy of cathode polarization were 0.57 and 0.22 eV

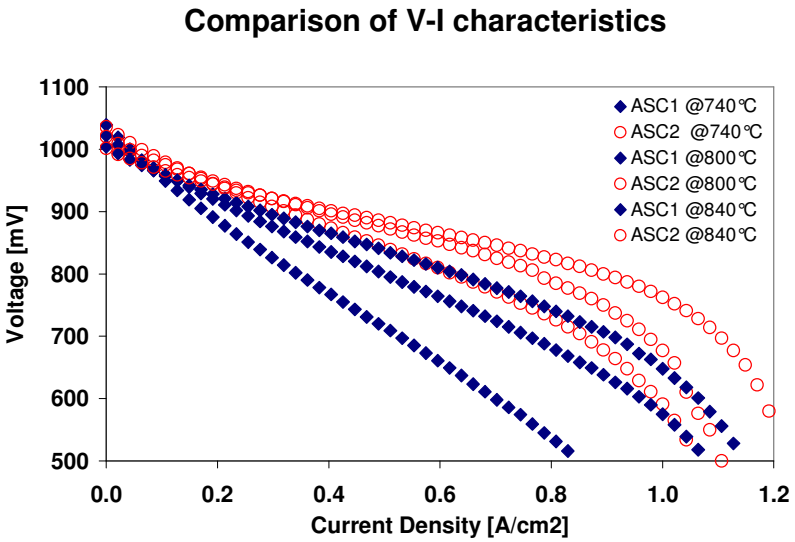

Figure 7. Comparison of ASC1 and ASC2 performances

respectively for ASC1 and ASC2. This means that for the ASC1 cell the activation polarization term is the limiting factor for lowering the operating temperature, while for ASC2 the limiting factor is the ohmic polarization.

5. CONCLUSIONS

In this paper an experimental analysis of solid oxide fuel cells was performed and was focused on the comparison of behavior of two anode supported cells with LSM (ASC1) and LSCF (ASC2) cathodes.

The current-voltage behavior of ASC2 at 740°C is comparable with performance of ASC2 at 840 °C. Further, at 740 °C the voltage of 0.7 volts is reached at a double value of current density in the case of ASC2.

The apparent thermal activation energy E_a has been evaluated from the temperature dependence of ASRs. The cell with LSCF cathode has a lower activation energy and it is possible to conclude that this cell is suitable for operating temperature lower than ASC1 cell. Further, for the ASC1 cell the activation polarization term is the limiting factor for lowering the operating temperature, while for ASC2 it is the ohmic polarization is the limiting factor.

ACKNOWLEDGMENTS

bla bla bla bla bla bla bla bla bla bla bla bla.

REFERENCES

[1]. T.M. Koehler, D.B. Jarrel, L.J. Bond, High Temperature Ceramic Fuel Cell Measurement and Diagnostics for application to Solid Oxide Fuel Cell Systems, Report prepared for the U.S. Department of Energy, October 2001.

[2]. Singhal S.C., Kendall K., High temperature solid oxide fuel cells: fundamentals, design and applications, Elsevier (2004).

[3]. Kim J., Virkar A.V., Fung K.Z., Metha K., Singhal S.C., Polarization effects in intermediate temperature, Anode-Supported Solid Oxide Fuel Cells, J. Electrochemical Soc., Vol. 146 (1), pp. 69-78 (1999).

[4]. Zhao F., Virkar A. V., Dependence of polarization in anode-supported solid oxide fuel cells on various cell parameters, Journal of Power Sources 141 (2005) 79–95.

[5]. H.Y. Jung, W.-S. Kim, S.-H. Choi, H.-C. Kim, J. Kim, H.-W-Lee, J.-H. Lee, Effect of current-collecting layer on unit-cell performance of anode-supported solid oxide fuel cells, J. Power Sources, 155 (2006) 145–151.

[6]. V.V. Srdic, R.P. Omorjan, J.Seidel, Electrochemical performances of $(La,Sr)CoO_3$ cathode for zirconia-based solid oxide fuel cells, Materials Science and Engineering B 116 (2005) 119–124.

[7]. V. Dusastre, J.A. Kilner, Solid State Ionics 126 (1999) 163.

[8]. A. Mai, V.A.C. Haanappel, S. Uhlenbruck, F. Tietz, D. Stover, Ferrite-based perovskites as cathode materials for anode-supported solid oxide fuel cells. Part I. Variation of composition, Solid State Ionics 176 (2005) 1341 – 1350.

[9]. F. Tietz ., V.A.C. Haanappel, A. Mai, J. Mertens, D. Stover, Performance of LSCF

[10]. B. Rietveld, Low Temperature SOFC for lifetime and reduced costs, Finnish SOFC Symposium, 29 June 2006.

[11]. Noren D.A., Hoffman M.A, Clarifying the Butler–Volmer equation and related approximations for calculating activation losses in solid oxide fuel cell models, Journal of Power Sources 152 (2005) 175–181

[12]. Reid R.C., Prausnitz J.M., Poling B., The properties of gases & liquids, Fourth Edition, McGraw-Hill, Inc., 1987.

[13]. Todd B., Young J.B., Thermodynamic and transport properties of gases for use in solid oxide fuel cell modeling, J. Power Sources, 110, 186–200 (2002).

Nomenclature

ASR	Area Specific Resistance (Ω cm^2)	R	universal gas constant (J mol^{-1} K^{-1})
$D_{i\text{-}j}$	Fundamental binary diffusivity in the electrode (cm^2/s)	R_Ω	Cell ohmic resistance (Ω cm^2)
$D_{a(eff)}$	Effective binary diffusivity in the anode layer (cm^2/s)	*SOFC*	Solid Oxide Fuel Cell
$D_{c(eff)}$	Effective binary diffusivity in the cathode layer (cm^2/s)	T	temperature (K)
E_a	Thermal activation energy (eV)	t_a	thickness of the anode layer (cm)
F	Faraday number (C mol^{-1})	t_c	thickness of the cathode layer (cm)
i_{as}	Anode limiting current (A cm^{-2})	V_c	Cell terminal voltage (V)
i_{cs}	Cathode limiting current (A cm^{-2})	V_{diff}	Diffusion overpotential (V)
i	Cell current density (A cm^{-2})	V_{Nernst}	Nernst potential (V)
I_{0_c}	Effective exchange current density (A cm^{-2})	*YDC*	Yttria Doped Ceria
LSCF	Lanthanum Strontium Cobalt Ferrite Oxide	*YSZ*	Yttria Stabilized Zirconia
LSM	Lanthanum Strontium Manganese Oxide	*Greek*	
MPD	Maximum Power Density (mW cm^{-2})	α	effective charge transfer coefficient
OCV	Open Circuit Voltage (V)	ε	electrode porosity
$p^b_{H_2}$	hydrogen pressure at the anode bulk (Pa)	ρ_{el}	Resistivity of electrolyte (Ω cm)
$p^b_{O_2}$	oxygen pressure at the cathode bulk (Pa)	τ	electrode tortuosity